Hindawi Publishing Corporation
Smart Materials Research
Volume 2012, Article ID 258638, 7 pages
doi:10.1155/2012/258638

Research Article

Magnetostrictive Actuation of a Bone Loading Composite for Accelerated Tissue Formation

Stephen Hart, Ryan Bucio, and Marcelo Dapino

Department of Mechanical & Aerospace Engineering, The Ohio State University, E307 Scott Laboratory, 201 West 19th Avenue, Columbus, OH 43210, USA

Correspondence should be addressed to Marcelo Dapino, dapino.1@osu.edu

Received 27 May 2011; Revised 28 September 2011; Accepted 2 October 2011

Academic Editor: Osama J. Aldraihem

When bone is dynamically loaded it adapts its shape to better support the load. We have developed a magnetostrictive composite consisting of Terfenol-D particles encapsulated in an epoxy resin that changes length when exposed to magnetic fields. When bonded to the surface of a porcine tibia *ex vitro*, the composite produces surface strains greater than 900 $\mu\varepsilon$ at a frequency of 30 Hz and magnetic field of 170 kA/m. This is more than sufficient strain magnitude and frequency to promote cortical bone growth in both rats and turkeys and to maintain cortical bone structure in humans. Key advantages of the composite over conventional electromechanical or thermomechanical actuators are its simplicity, compact size, and remote actuation. A mathematical model describing the strains and stresses in the bone is presented.

1. Introduction

Bone structure continuously evolves by building new bone and resorbing old bone [1]. The dynamic property of bone remodeling allows bone tissue to adapt to changes in its loading environment [2]. Although the exact mechanism explaining bone remodeling remains elusive, interstitial fluid flow around a particular subset of bone cells called osteocytes is thought to be essential [3]. Eccentric loading of a long bone creates a bending moment and causes the bone to curve. This creates a region of tension on one side of the bone and a region of compression on the opposite side. As the load is cycled, interstitial fluid flows around osteocytes from regions of compression to regions of tension resulting in shear stress on the cell walls. Shear stress is thought to incite a molecular cascade resulting in new bone growth [4, 5].

In humans, strains below 200 $\mu\varepsilon$ do not stimulate cortical bone remodeling [6]. Strain values between 200 and 2000 $\mu\varepsilon$ represent physiological levels of strain on the human skeleton. Above 2000 $\mu\varepsilon$, the rate of bone formation exceeds the rate of bone resorption, and growth is observed [7]. Studies involving turkeys have shown that a 30 Hz, 100 $\mu\varepsilon$ signal is sufficient to maintain bone mass [8], and studies involving rats have shown that a 2 Hz, 930 $\mu\varepsilon$ signal is sufficient to produce bone growth [9]. Along with strain magnitude, the strain rate plays an important role in new bone formation [10]. Based on a compilation of previous studies where animal bones were subjected to mechanical loads *in vivo*, Turner [11] and Burr et al. [12] concluded that the strain rate and magnitude are related to the strain stimulus by

$$S = k\varepsilon f, \tag{1}$$

where S is the strain stimulus, k is a proportionality constant, ε is the strain magnitude, and f is the strain frequency. The strain stimulus induced in bone as a result of oscillating bending stresses is directly proportional to both the magnitude and frequency of the strain signal. This relationship implies that the strain frequency modulates the effect of mechanical loading on bone tissue formation and the minimum strain magnitude required to stimulate bone tissue formation decreases with increasing frequency. It has been shown in a study involving an avian ulna that 500 $\mu\varepsilon$ applied at 1 Hz has little effect on bone, but is highly osteogenic if the frequency is increased to between 10 and 60 Hz. Studies have shown that strains as low as two orders of magnitude below physiological levels can induce large increases in bone mass if applied at 30 Hz [2, 10, 13].

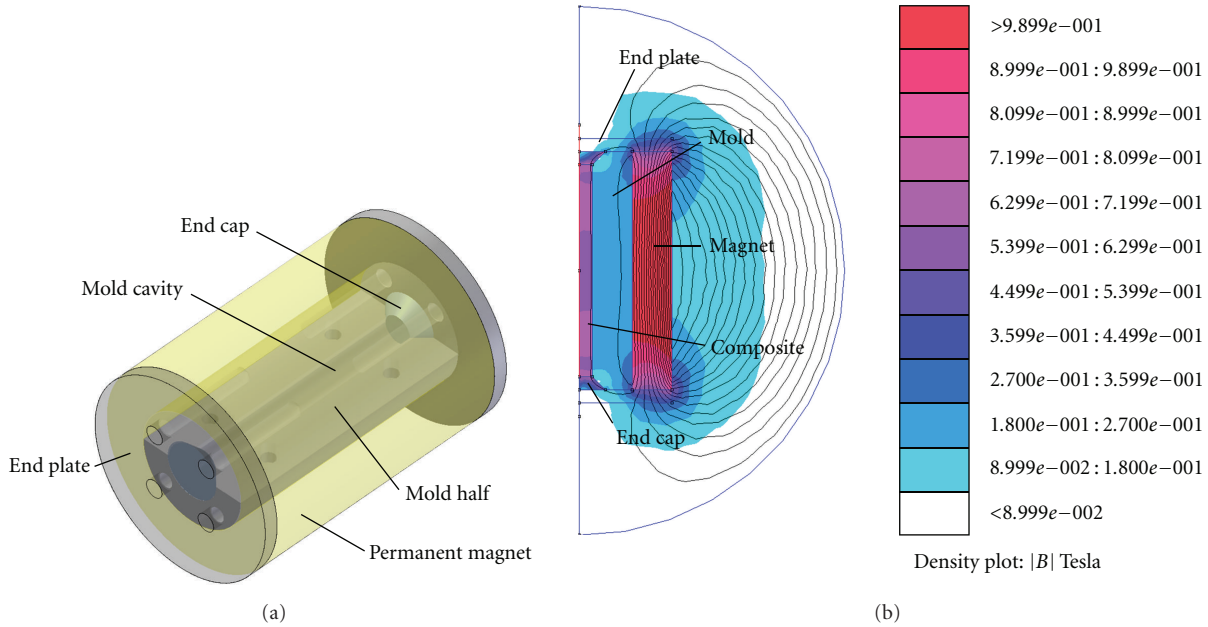

Figure 1: (a) Casting mold with permanent magnet in position; (b) finite element model of the magnetic circuit.

This paper is focused on the development of an implantable magnetostrictive composite material able to mechanically load bone samples *ex vitro*, with remote actuation, to strain levels shown in the literature to accelerate tissue formation *in vivo*.

Magnetostrictive materials exhibit a change in length and material properties when placed in a magnetic field [14]. By rigidly attaching a magnetostrictive material to the shaft of a long bone and placing the system in an alternating magnetic field, the magnetostrictive material's length will oscillate creating dynamic bending stress through the cross-section of the bone.

Terfenol-D (terbium-dysprosium-iron) is the most advanced commercially available magnetostrictive material [15]. Monolithic Terfenol-D exhibits a relatively large static strain magnitude of 1600 $\mu\varepsilon$, but is brittle and is prone to frequency-dependent losses. Magnetostrictive composites consisting of Terfenol-D powder dispersed in an epoxy matrix can overcome the intrinsic brittleness of Terfenol-D while potentially enabling biocompatibility through the use of an appropriate matrix.

2. Methods

2.1. Magnetostrictive Composite. In this study, Derakane 411-C-50 epoxy vinyl ester resin (viscosity 112 cSt, tensile modulus 0.49 Mpsi, compressive modulus 0.35 Mpsi) was used as a binder because of its low modulus of elasticity, which minimizes magnetostriction loss. Methyl ethyl ketone peroxide (MEKP) was used as the catalyst for the epoxidation reaction, and Cobalt naphthenate (CoNap) was the reaction promoter. The binder was mixed in a 97.8% resin, 2.0% MEKP, and 0.2% CoNap ratio by mass. The Terfenol-D particles (ETREMA Products Inc., Ames, IA) were manufactured by a ball-milling process producing low-aspect-ratio particles ranging in size from 106 to 300 microns oriented along the [112] axis. The composite was mixed in an open-air container with the appropriate amount of Terfenol-D particulate to achieve an approximately 50% volume fraction between the resin and the Terfenol-D. While casting the sample in a vacuum would have aided in the elimination of air pockets within the matrix, it has been shown that the performance of the vacuum-cast composite is comparable to that achievable through open-air casting [16]. The mixed resin/Terfenol-D particles were cast in an aluminum mold sealed with silicon (Figure 1(a)). A nickel-plated neodymium iron boron (NdFeB) magnet designed to produce a longitudinal magnetic field of 140 kA/m was quickly slid over the mold to align the particles during the composite cure and prevent the particles from settling towards the bottom of the mold (Figure 1(b)).

To ensure a complete cure, the composite and mold were placed in a convection oven at 343 K for 6 hours. Following the cure, the composite was machined to achieve squared ends. The composite sample was then cut into rods of approximate dimensions 0.0254 m (length) by 0.00635 m (diameter). One piece was used for microscopy, and the other was cut in half along the longitudinal axis to create a semicylindrical geometry able to be bonded to the bone sample.

Scanning electron microscopy was used to investigate the distribution and orientation of the particles within the cured composite. The semicylindrical sample was mounted in conductive Bakelite as shown in Figure 2 along the long axis of the composite rod. The exposed surface was then polished on a vibratory polisher for 48 hours. Scanning electron microscopy was performed using a back-scatter detector (BSD).

Figure 2: Axial cross-section of Terfenol-D composite mounted in conductive Bakelite.

The procedure to calculate the volume fraction for each sample was as follows. The SEM images showed no voids; hence voids were assumed negligible. First, we estimated mixture volume including the mold volume and waste volume (V_M) and the desired volume fraction of Terfenol-D (vf_T). We then estimated the mass of Terfenol-D powder required (m_{TR}) and resin required (m_{RR}) in grams by multiplying the volumes by the material densities,

$$\begin{aligned} m_{\mathrm{TR}} &= 9.21\frac{\mathrm{g}}{\mathrm{mL}}(vf_T \times V_M)\mathrm{mL}, \\ m_{\mathrm{RR}} &= 1.045\frac{\mathrm{g}}{\mathrm{mL}}((1 - vf_T) \times V_M)\mathrm{mL}. \end{aligned} \tag{2}$$

After adding (m_{RR}) of Derakane resin to the mixing container (m_C), we calculated the actual mass of resin in the mixing container (m_{Resin}). We then calculated the mass of MEKP (m_{MEKP}) in grams and CoNap (m_{CoNap}) in grams required for the resin and calculated the actual amount of mixed resin used (m_E). The mass of Terfenol-D powder in grams required to achieve the desired volume fraction based on the actual amount of resin mixed is

$$m_{\mathrm{TR}} = m_E\left(\frac{vf_T}{1 - vf_T}\right)\left(\frac{9.21}{1.045}\right), \tag{3}$$

whereas the actual amount of Terfenol-D added to the mixing container is (m_T). After the composite has been cast and cured, we calculated the final volume fraction of Terfenol-D achieved in the composite as

$$VF_T = \frac{m_T/9.21}{m_T/9.21 + m_E/1.045}. \tag{4}$$

2.2. Drive Coil. A 2400-turn coil constructed from 20 AWG magnet wire was fabricated in order to drive the composite and generate strain. A two-layer pick-up coil was placed inside the drive coil to measure the magnetization of the composite. The drive coil has a resistance of 18.9 Ω and a field rating of 1.6×10^3 A/m/V. The drive coil was driven by two Techron Model 8524 Gradient Drive amplifiers (Elkhart, IN) connected in series. The setup was controlled with a Data Physics SignalCalc Mobilyzer dynamic analyzer connected to a personal computer.

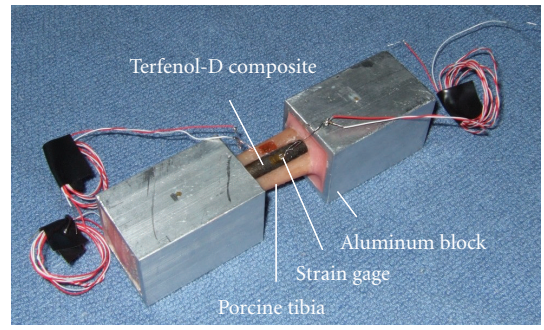

Figure 3: Composite and bone system.

2.3. Magnetostrictive Composite-Bone Test Setup. To measure the unloaded magnetostriction, the Terfenol-D composite was tested in the drive coil before it was bonded to the bone sample. The composite was placed in a nonmagnetic spacer to ensure alignment of the composite through the center of the coil. Current through the coil was increased in a stepwise fashion until the maximum operating temperature of the coil was reached (100°F). The drive coil was driven at a frequency of 30 Hz for all tests.

A right tibia from a mature porcine was chosen for the relatively flat surface it provides on the posterior aspect inferior to the tibial plateau for bonding the magnetostrictive composite. In addition, the porcine tibia was appropriate because the mechanical properties of bone tissue among most mammals are similar, with the major difference being bone size [1]. The average elastic modulus of the specimen is approximately 3 MPa and that of a human tibia is 5.44 MPa [17]. The sample was cleared of all soft tissue to attain a clean specimen of bone. The bone ends were potted in aluminum blocks using polymethylmethacrylate to facilitate mechanical testing, as shown in Figure 3. The bone sample had exposed dimensions of 0.031 m × 0.0173 m × 0.01375 m. The semi-cylindrical composite was applied along the long axis of the bone with cyanoacrylate glue. Strain was measured with two strain gages. The first gage was bonded to the composite and the second to the bone surface adjacent to the composite. The bone was then slid into the drive coil for testing with free-free boundary conditions.

3. Results

3.1. Terfenol-D Composite. The final volume fraction of Terfenol-D was calculated at 50.2%. Figure 4 demonstrates particle distribution along the long axis of the composite. The particles appear evenly and randomly distributed. No voids were observed in the resin mixture.

Dynamic unconstrained tests (prior to bonding) of the Terfenol-D composite with free-free boundary conditions were conducted at fields ranging from 110 kA/m to 170 kA/m (with equal magnetic bias) at a frequency of 30 Hz. As

Table 1: Terfenol-D composite and bone surface strain values (peak-peak).

Experimental Terfenol-D composite strain ($\mu\varepsilon$)	Experimental and FEA Bone surface strain: adjacent to composite ($\mu\varepsilon$)	FEA Bone surface strain: opposite to composite ($\mu\varepsilon$)
2200	~930	390

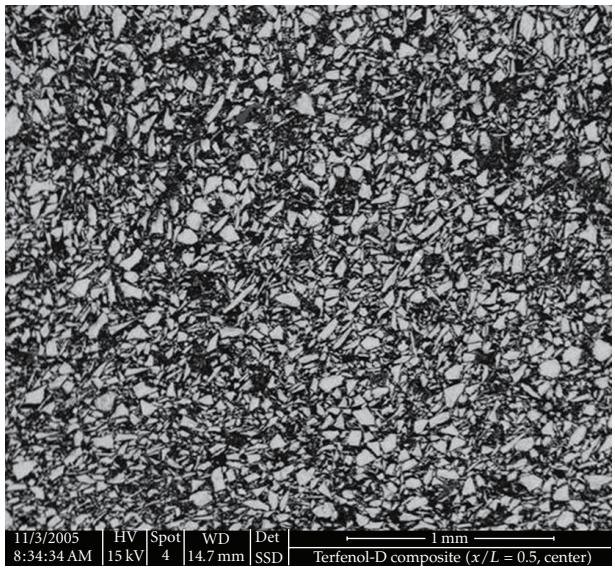

Figure 4: Axial cross-section of Terfenol-D composite.

the field intensity was increased, the dynamic strain produced in the Terfenol-D composite also increased to a maximum of 2300 $\mu\varepsilon$ peak-peak (Figure 5). The increasing trend in magnitude indicates that saturation magnetostriction was not achieved over this range of fields, but fields higher than 170 kA/m were not possible on this system at 30 Hz due to excessive heating of the drive coil.

3.2. Bone Loading Experiments and Calculations. The composite was subsequently bonded to the bone and driven at 30 Hz at 170 kA/m, and equal magnetic bias. The strain values measured along the longitudinal axis are shown in Table 1. The maximum experimental peak-peak strain achieved on the composite surface was 2200 $\mu\varepsilon$, which almost coincides with the unloaded strain, suggesting that the top surface displaces almost freely relative to the surface in contact with the bone.

A finite element model was developed which consists of a three-dimensional COMSOL Multiphysics simulation for the bone sample. The simulated bone sample had dimensions of $0.031 \times 0.0173 \times 0.01375$ m and a radius of .003 m along the edges. The model had fixed end conditions, and an input displacement was applied on the rectangular surface where the Terfenol-D composite would excite the bone structure. This displacement input was set to coincide with the unloaded deformation measured from the Terfenol-D element. The center of the model experienced zero displacement, and the two ends of the rectangular area experienced maximum displacement (Figure 6). The modeled displacement closely matches the longitudinal, z-direction, and magnetostriction strain measured on the surface adjacent to the rectangular area (930 $\mu\varepsilon$). As shown in Table 1, the strain on the surface adjacent to the composite has a larger strain magnitude than the surface opposite the composite. The induced strain distributions on the bone surface are shown in Figure 7.

3.3. System Model. A continuum model for the active system was implemented as illustrated in Figure 8. The composite is at the top, and the bone is at the bottom, with an adhesive layer between the two. Since the cyanoacrylate that was used to bond the composite to the bone is viscoelastic, a shear loss results between the Terfenol-D and the bone.

Linear modeling of the composite begins with the constitutive piezomagnetic relation for strain [14],

$$\varepsilon = \frac{\sigma^H}{E^H} + qH, \tag{5}$$

where ε is the total strain, σ is the axial stress induced by the applied magnetic field H, E^H is the Young's modulus at constant magnetic field, and q is the axial strain coefficient. A q value of 2.71×10^{-6} m/A is used. The shear stress developed at the interface between the composite and adhesive is given by

$$\tau_{T-D} = \frac{E^H \varepsilon A_c}{A_{T-D/\text{Adhesive}}}, \tag{6}$$

where A_c is the cross-sectional area of the composite and $A_{T-D/\text{Adhesive}}$ is the area of the composite/adhesive interface.

The adhesive layer is modeled as a spring and damper system in parallel, which results in a complex shear modulus of the form

$$G_A = k + ib(\omega), \tag{7}$$

where k is the real component of the modulus and b is a damping coefficient. In addition to relation (7), the complex shear modulus may be described as a ratio of G_{diss} to G_{store} representing the dissipated (imaginary) and storage (real) moduli, respectively. This ratio is also referred to as the "loss" factor,

$$G_A = \frac{G_{\text{diss}}}{G_{\text{store}}}. \tag{8}$$

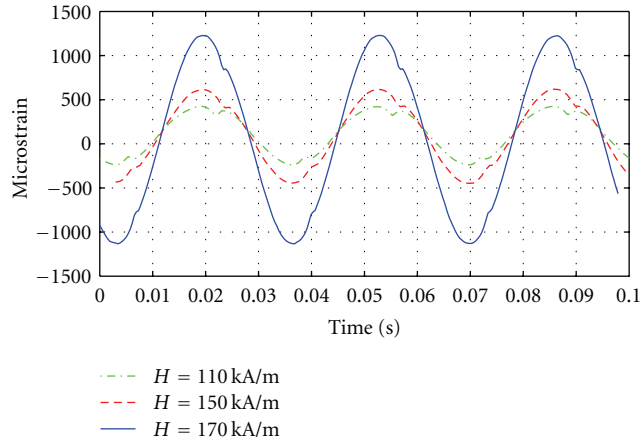

Figure 5: Unconstrained Terfenol-D composite dynamic tests at $f = 30$ Hz with varying field intensity.

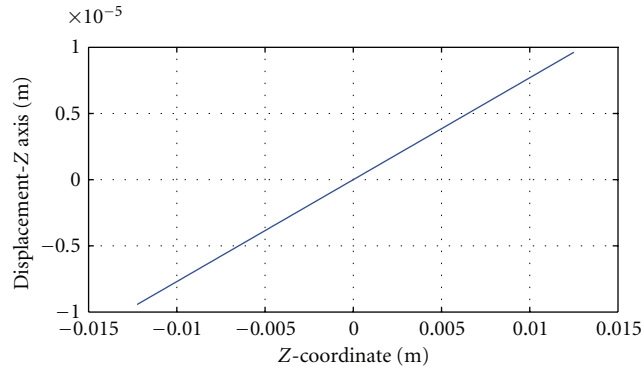

Figure 6: Model for the applied displacement on the bone surface where the Terfenol-D element would excite the bone structure.

The force and strain applied to the bone may be described by

$$F_b = \tau_b w \int dl,$$
$$\varepsilon_b = \frac{F_b}{E_b A_b}, \tag{9}$$

where F_b is the force exerted by the bone on the deforming composite, τ_b is the shear stress developed on the bone surface, w is the width of the adhesive/bone interface, dl is the differential length along the adhesive/bone interface, ε_b is the strain developed on the bone surface, E_b is the modulus of elasticity for the bone, and A_b is the cross-sectional area of the bone. A comparison between model calculations and measured strain on the bone adjacent to the composite is shown in Figure 9. We note that use of the linear piezomagnetic equation for strain is justified in the fact that the composite is biased with a magnetic field, yielding quasilinear responses for the Terfenol-D phase. As evidenced by the accurate model results shown in Figure 9, the overall response of the composite can be adequately approximated with linear behavior for the combined Terfenol-D and linearly elastic matrix.

4. Discussion

This study demonstrates that a magnetostrictive composite bonded to the surface of a long bone is able to produce surface strains in the physiological range for humans. A maximum peak-peak strain of 930 $\mu\varepsilon$ was measured on the surface of the bone sample when driving the coil at a frequency of 30 Hz. This measurement is reasonable as dynamic effects are significant at this frequency considering that the natural frequency of the system is approximately 60 Hz. The drive frequency of 30 Hz was chosen based on previous literature, but according to (1), driving the coil at higher frequencies would further increase the strain stimulus. The initial unconstrained tests indicate that saturation was not achieved. If the drive coil was redesigned to address ohmic heating limitations, the coil could be operated at higher field ratings producing additional magnetostriction.

The strain magnitude measured on the bone surface adjacent to the composite is less than that of the composite itself. This loss in strain is attributed to the constrained boundary conditions (bonded to bone) and the viscoelastic nature of the adhesive used to bond the composite to the bone.

Microscopic analysis demonstrated that open-air casting results in a uniform distribution of Terfenol-D particles.

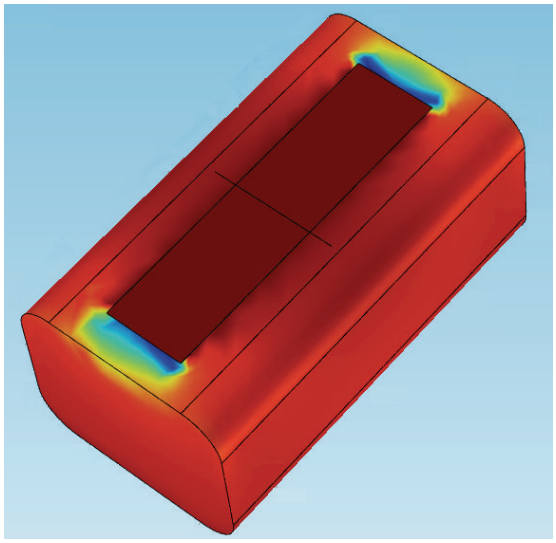

Figure 7: Strain distribution along longitudinal direction of FEA bone model.

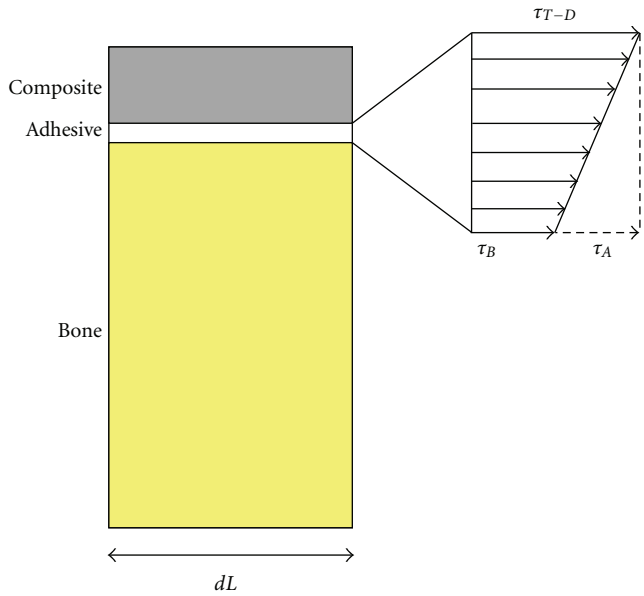

Figure 8: Differential continuum model of the composite, adhesive, and bone system.

The particles did not appear to be aligned in "columns" as described elsewhere [18]. However, the composite was cured under a magnetic field resulting in parallel orientation of the crystalline structures along the long axis of the composite.

The strong correlation between the predicted and actual strain indicates that this model can be used to accurately determine the strain levels in other long bones stimulated by a similar Terfenol-D composite. This conceptual frame work can be used to optimize custom system parameters needed to promote bone tissue formation for specific applications.

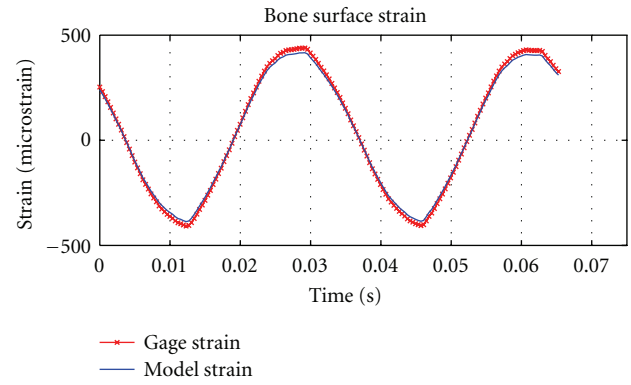

Figure 9: Predicted strain from model versus gage strain on the bone surface.

To hasten fracture healing, the composite could be used to apply cyclic compressive strains around the fracture callus to increase the bone formation rate reducing rehabilitation time [19]. The Terfenol-D composite could also be applied to patients experiencing disuse atrophy to form stronger and thicker periosteal surfaces to help prevent bone fractures [20]. Astronauts and pilots routinely subjected to minimum gravity environments could also benefit from mechanical loading to prevent bone atrophy. The symptoms of osteoporosis might also be diminished if a useful mechanism for bone strengthening is created. For *in vivo* applications, the Terfenol-D composite could be actuated remotely by a coil wrapped around a limb or body part.

A number of bone "fusion" devices and bone-lengthening devices exist but are cumbersome and often painful to the wearer. Ankle and foot arthrodesis is aided by an implantable device that produces an electrical signal to the bone (OsteoGen, Biomet Inc.) [21, 22]. Spinal bone stimulation devices (SpinalPak, Biolectron, Inc. and Spinal-Stim Lite, Orthofix, Inc.) utilize external electrical or magnetic fields to the desired location. A fully implantable spinal fusion stimulator (SpF, Biomet Inc.) is available in several configurations and consists of a direct current generator with a lithium iodine battery. Bone-lengthening devices using screws, gearboxes, and springs have also proliferated [23]. These devices, however, focus on fusing two different bones or lengthening bone. The concept provided in this study focuses on making bone stronger.

Although the results from this study are positive, this design is subject to biological and structural limitations that must be investigated. Similar to other implantable bone growth stimulators, the application of this composite to the surface of a long bone requires surgery, and the biocompatibility of the Terfenol-D composite system has yet to be determined. Also, applying the composite to the periosteal surface of a long bone may itself cause a periosteal response and reduce the adhesion of the composite to the bone. The effectiveness of the Terfenol-D composite to stimulate bone tissue formation will need to be determined through *in vivo* testing.

Conflict of Interest

S. Hart, R. Bucio, and M. Dapino report no conflict of interest with this study.

Acknowledgments

The authors wish to acknowledge Dr. Njus of the Department of Biomedical Engineering at the University of Akron, who provided the porcine tibia used in this study, and Cameron Begg, Department of Materials Science and Engineering, Ohio State University who provided microscopy assistance. They would also like to thank Robert Siston, Department of Mechanical and Aerospace Engineering at the Ohio State University for useful suggestions. This study was funded by the Ohio State University College of Engineering.

References

[1] A. G. Robling, A. B. Castillo, and C. H. Turner, "Biomechanical and molecular regulation of bone remodeling," *Annual Review of Biomedical Engineering*, vol. 8, no. 1, pp. 455–498, 2006.

[2] P. J. Ehrlich and L. E. Lanyon, "Mechanical strain and bone cell function: a review," *Osteoporosis International*, vol. 13, no. 9, pp. 688–700, 2002.

[3] E. M. Aarden, E. H. Burger, and P. J. Nijweide, "Function of osteocytes in bone," *Journal of Cellular Biochemistry*, vol. 55, no. 3, pp. 287–299, 1994.

[4] C. H. Turner, M. R. Forwood, and M. W. Otter, "Mechanotransduction in bone: do bone cells act as sensors of fluid flow?" *The FASEB Journal*, vol. 8, no. 11, pp. 875–878, 1994.

[5] C. H. Turner and F. M. Pavalko, "Mechanotransduction and functional response of the skeleton to physical stress: the mechanisms and mechanics of bone adaptation," *Journal of Orthopaedic Science*, vol. 3, no. 6, pp. 346–355, 1998.

[6] H. M. Frost, "A proposed pathogenically adaptive bone remodeling," *Journal of Biomechanics*, vol. 2, pp. 73–85, 1987.

[7] K. Khan, H. McKay, P. Kannus, D. Bailey, J. Wark, and K. Bennell, *Physical Activity and Bone Health*, Human Kinetics, Champaign, Ill, USA, 2001.

[8] Y. X. Qin, C. T. Rubin, and K. J. McLeod, "Nonlinear dependence of loading intensity and cycle number in the maintenance of bone mass and morphology," *Journal of Orthopaedic Research*, vol. 16, no. 4, pp. 482–489, 1998.

[9] C. H. Turner, M. R. Forwood, J. Y. Rho, and T. Yoshikawa, "Mechanical loading thresholds for lamellar and woven bone formation," *Journal of Bone and Mineral Research*, vol. 9, no. 1, pp. 87–97, 1994.

[10] J. R. Mosley and L. E. Lanyon, "Strain rate as a controlling influence on adaptive modeling in response to dynamic loading of the ulna in growing male rats," *Bone*, vol. 23, no. 4, pp. 313–318, 1998.

[11] C. H. Turner, "Three rules for bone adaptation to mechanical stimuli," *Bone*, vol. 23, no. 5, pp. 399–407, 1998.

[12] D. B. Burr, A. G. Robling, and C. H. Turner, "Effects of biomechanical stress on bones in animals," *Bone*, vol. 30, no. 5, pp. 781–786, 2002.

[13] Y. F. Hsieh and C. H. Turner, "Effects of loading frequency on mechanically induced bone formation," *Journal of Bone and Mineral Research*, vol. 16, no. 5, pp. 918–924, 2001.

[14] M. J. Dapino, "On magnetostrictive materials and their use in adaptive structures," *Structural Engineering and Mechanics*, vol. 17, no. 3-4, pp. 303–329, 2004.

[15] N. Nersessian, S. W. Or, and G. P. Carman, "Magneto-thermo-mechanical characterization of 1–3 type polymer-bonded Terfenol-D composites," *Journal of Magnetism and Magnetic Materials*, vol. 263, no. 1-2, pp. 101–112, 2003.

[16] T. A. Duenas and G. P. Carman, "Particle distribution study for low-volume fraction magnetostrictive composites," *Journal of Applied Physics*, vol. 90, no. 5, pp. 2433–2439, 2001.

[17] K. Choi, L. J. Kuhn, M. J. Ciarelli, and S. A. Goldstein, "The elastic moduli of human subchondral, trabecular, and cortical bone tissue and the size-dependency of cortical bone modulus," *Journal of Biomechanics*, vol. 23, no. 11, pp. 1103–1113, 1990.

[18] X. Dong, M. Qi, X. Guan, and J. Ou, "Microstructure analysis of magnetostrictive composites," *Polymer Testing*, vol. 29, no. 3, pp. 369–374, 2010.

[19] E. F. Morgan, R. E. Gleason, L. N. M. Hayward, P. L. Leong, and K. T. Salisbury Palomares, "Mechanotransduction and fracture repair," *The Journal of Bone and Joint Surgery A*, vol. 90, supplement 1, pp. 25–30, 2008.

[20] J. Charnley, "Anchorage of the femoral head prosthesis to the shaft of the femur," *The Journal of Bone and Joint Surgery B*, vol. 42, pp. 28–30, 1960.

[21] R. T. Hockenbury, M. Gruttadauria, and I. McKinney, "Use of implantable bone growth stimulation in charcot ankle arthrodesis," *Foot and Ankle International*, vol. 28, no. 9, pp. 971–976, 2007.

[22] A. Saxena, L. A. DiDomenico, A. Widtfeldt, T. Adams, and W. Kim, "Implantable electrical bone stimulation for arthrodeses of the foot and ankle in high-risk patients: a multicenter study," *The Journal of Foot and Ankle Surgery*, vol. 44, no. 6, pp. 450–454, 2005.

[23] P. Sharke, "The machinery of life," *Mechanical Engineering*, vol. 126, no. 2, pp. 30–34, 2004.